

Nonequilibrium surface growth in a hybrid inorganic-organic system

Nicola Kleppmann and Sabine H. L. Klapp

Institut für Theoretische Physik, Technische Universität Berlin, Hardenbergstrasse 36, 10623 Berlin, Germany

(Received 2 November 2015; published 15 December 2016)

Using kinetic Monte Carlo simulations, we show that molecular morphologies found in nonequilibrium growth can be strongly different from those at equilibrium. We study the prototypical hybrid inorganic-organic system 6P on ZnO(10 $\bar{1}$ 0) during thin film adsorption, and find a wealth of phenomena, including reentrant growth, a critical adsorption rate, and observables that are nonmonotonous with the adsorption rate. We identify the transition from lying to standing molecules with a critical cluster size and discuss the competition of time scales during growth in terms of a rate-equation approach. Our results form a basis for understanding and predicting collective orientational ordering during growth in hybrid material systems.

DOI: [10.1103/PhysRevB.94.241404](https://doi.org/10.1103/PhysRevB.94.241404)

Hybrid inorganic-organic systems (HIOSs) have revolutionized optoelectronic semiconductor technologies by combining the high charge carrier densities and high tunability of conjugated organic molecules with stable, well controlled inorganic substrates [1,2]. At the same time, the design of efficient devices poses fundamental physical questions on a multitude of length and time scales, from resonance energy transfer in complex environments [3–6] and energy level alignment [7,8] to classical statistical physics problems such as collective ordering of anisotropic molecules at interfaces, both in equilibrium and during nonequilibrium growth, i.e., at finite flux [9–11]. The final orientational ordering is indeed crucial for HIOS functionality [9]. Experimentally, a number of interesting structural phenomena in HIOSs have been observed, such as an increase of lying clusters with temperature [12], the coexistence of domains with different molecular tilt angles, and layer-dependent tilt angles [13]. However, so far there is no consistent understanding from the theoretical side [9,14]. A generic, yet unsettled, phenomenon seems to be that single molecules lie on substrates, while thin films generally form a standing configuration. Understanding this transition is further challenged by the fact that in a typical HIOS, the substrate generates electrostatic or topological surface fields with a significant impact on molecular ordering [11].

In the present Rapid Communication, we consider a *prototypical* HIOS system and ask the following question: How does the molecular component transition from lying molecules to standing clusters during nonequilibrium, submonolayer growth? We demonstrate, using theoretical calculations, that this transition is dominated by an interplay of anisotropic interactions and growth kinetics.

Specifically, we consider sexiphenyl (6P) molecules on a zinc-oxide (ZnO) 10 $\bar{1}$ 0 surface (see Fig. 1). This system combines two generic HIOS features: strongly anisotropic molecules with nonsymmetric (here dominantly quadrupolar) charge distributions and an electrostatically patterned substrate, here “charge stripes” [4]. We have recently developed a coarse-grained model [15] based on density functional theory (DFT) parametrization [16,17], which reproduces key equilibrium properties. Here, we employ kinetic Monte Carlo (KMC) simulations to access the large time and length scales of collective ordering for different adsorption rates. Currently, KMC simulations of anisotropic molecules are in their infancy. One conceptual problem is that the molecules’ mobility is

influenced by its orientation [18–20]. In earlier studies of molecular growth, the molecules’ orientations are strongly restricted to discrete orientations [21–23] or a two-dimensional (2D) (stripe-patterned) plane [18]. However, in reality most organic molecules explore the full, three-dimensional (3D) space of orientations [9,12]. Here, we consider molecules that are translationally confined to a 2D lattice, but have continuous, 3D rotational degrees of freedom. As very few growth simulations of hybrid systems exist, and since 6P/ZnO(10 $\bar{1}$ 0) forms a prototypical case, our results provide steps towards a general understanding of growth phenomena in HIOSs.

In KMC simulations, the surface evolution is described as a series of transitions between discrete states, where each transition is characterized through a rate. Specifically, we use a “composition and rejection” algorithm to select events and determine the system time from event propensities, a method previously used for biochemical models [24,25]. This algorithm is advantageous for simulations of molecules with both attractive and repulsive interactions and continuous rotational degrees of freedom, as it does not require the computationally expensive calculation of a complete process rate catalog after each process [26]. The processes occurring during surface growth can be summarized in terms of three different types, rotational diffusion (r), translational diffusion (d), and adsorption (a), described through the rates r_i^r , r_i^d , and r_i^a , respectively [see Fig. 1(a)]. Each process type is associated with an attempt frequency ν , which we use as propensity in our algorithm.

The rotational rate allows continuous rotational degrees of freedom. Using an adiabatic approximation, it can be expressed as

$$r_i^r = \nu^r \min\{\exp[\beta(H^i(i) - H^f(i))], 1\}, \quad (1)$$

where $H^i(i)$ and $H^f(i)$ are the effective coarse-grained interaction Hamiltonians for the initial and final configuration of molecule i , respectively, and $\beta = (k_B T)^{-1}$ is defined through the Boltzmann constant k_B and the temperature T . Here, we set $T = 300$ K. Following Ref. [15], the effective interaction Hamiltonian is written as

$$H_{\text{eff}}^{\text{pot}} = H_{\text{m-m}} + H_{\text{m-s}}, \quad (2)$$

where $H_{\text{m-m}}$ characterizes the intermolecular (6P-6P) interactions consisting of an electrostatic quadrupolar contribution

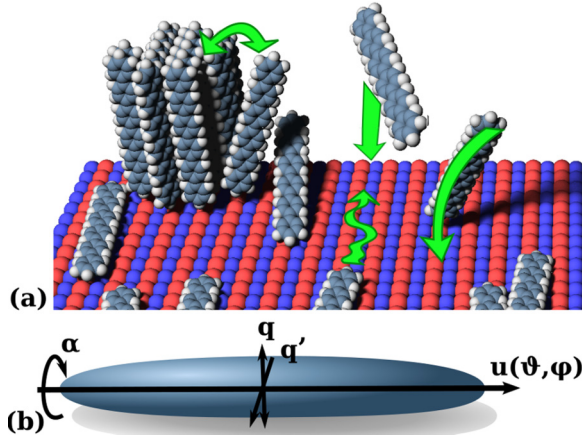


FIG. 1. Growth schematic for submonolayer growth of 6P on ZnO(10 $\bar{1}$ 0). (a) depicts the substrate (alternating blue and red colors represent charge lines) with molecules adsorbing, diffusing translationally and rotationally (see green arrows). (b) defines the three principal axes of a molecule, \mathbf{u} , \mathbf{q} and \mathbf{q}' , as a function of the three Euler angles α , ϑ , and φ (with \mathbf{q} and \mathbf{q}' defining linear quadrupole moments).

V_{QQ} [27] between the (linear) quadrupoles assigned by \mathbf{q} in Fig. 1(b) and a nonelectrostatic Gay-Berne interaction V_{GB} [17,28,29]. Correspondingly, the molecule-substrate Hamiltonian $H_{\text{m-s}}$ contains a quadrupole-field interaction for a quadrupole denoted by \mathbf{q}' in Fig. 1(b). This electrostatic interaction reflects the hybrid nature of the 6P/ZnO(10 $\bar{1}$ 0) system. A single 6P molecule tends to *align* with the charge lines of the substrate [12,16]. Further, $H_{\text{m-s}}$ includes a nonelectrostatic interaction V_{LJ} [30] that involves attractive z^{-3} interactions between a molecule and the substrate. The different contributions to $H_{\text{eff}}^{\text{pot}}$ are parametrized based on DFT calculations [15–17].

The rotational rate in Eq. (1) lacks transitional information between the initial and final configuration. This reflects the underlying “adiabatic” approximation, i.e., a much faster relaxation of rotational versus translational motion. The latter is modeled as an activated process between identical, *energetically most favorable* lattice sites of the ZnO(10 $\bar{1}$ 0) substrate [15], as discussed in detail in Ref. [31], Sec. I. As translational diffusion does not include any rotation, the m-s interaction of the initial site and destination are identical. Thus, r_i^{d} involves a constant contribution E_{d} determined through the substrate, as well as the initial neighbor interaction energy $H_{\text{m-m}}^{\text{i}}$,

$$r_i^{\text{d}} = \nu^{\text{d}} \begin{cases} \min\{\exp[\beta(H_{\text{m-m}}^{\text{i}}(i) - E_{\text{d}})], 1\}, & \text{if } H_{\text{m-m}}^{\text{f}}(i) \leq E_{\text{d}}, \\ \min\{\exp[\beta(H_{\text{m-m}}^{\text{i}}(i) - H_{\text{m-m}}^{\text{f}}(i))], 1\}, & \text{else.} \end{cases} \quad (3)$$

The second case comes into play if the molecule’s destination is blocked through a repulsive interaction with other molecules, i.e., if $H_{\text{m-m}}^{\text{f}}(i) > E_{\text{d}}$ [31].

In principle, information about E_{d} can be obtained from atomistically resolved molecular dynamics (MD) simulations [32]. These have shown that E_{d} is direction dependent (as one might expect). Nevertheless, we here set $E_{\text{d}} = 0$ eV for all directions of diffusion. Test calculations for $E_{\text{d}} \leq 0.2$ eV (the

free-energy barrier found for diffusion along charge lines [32]) indicate that this approximation has no substantial influence on our results.

The final process is the adsorption of molecules, expressed through the adsorption rate

$$r_i^{\text{a}} = \nu^{\text{a}} = f \nu^{\text{d}}. \quad (4)$$

Note that we do not consider desorption and only count particles that adsorb on previously *unoccupied* substrate sites. The numerical results presented below have been obtained using a vertical adsorption orientation of molecules; the influence of different adsorption configurations is discussed in Ref. [31], Sec. II. We use adsorption rates in the range of $10^{-6} \leq f \leq 1$, which we compare to the upper limit of the free diffusion rate $r_{\text{max}}^{\text{d}} \approx 2 \times 10^9$ Hz determined on the basis of MD simulations [32]. We find that for $f = 10^{-6}$ maximally half a monolayer of molecules adsorbs within ≈ 0.4 ms; thus we are far beyond the typical time scales of MD simulations. Simulation details are discussed in Ref. [31], Sec. I.

We characterize the orientational order using the order parameter tensor [33,34] $A_{\alpha\beta}(t) = N^{-1} \sum_{i=1}^N \langle u_{i,\alpha} u_{i,\beta} - \frac{1}{3} \delta_{\alpha\beta} \text{Tr}(\mathbf{u}_i \otimes \mathbf{u}_i) \rangle$, where Tr stands for the trace, \otimes denotes a dyadic product, and $\langle \dots \rangle$ is an average over all molecules and all runs in the system at time t . The nematic order parameter $S \in [-0.5, 1]$ and the biaxiality parameter $B \in [0, 1]$ are derived from the eigenvalues of $A_{\alpha\beta}(t)$ [31]. For a perfectly uniaxial system $S = 1$, $B = 0$, while $S = B = 0$ represents a completely disordered system. Positive values of both S and B indicate nematic ordering with some degree of biaxiality. Finally, molecular ordering along two orthogonal axes within a plane [35,36] yields $S = -\frac{1}{2}$, $B = 0$, corresponding to maximal biaxiality (for further details, see Ref. [31], Sec. III).

As a starting point, we consider the density of molecules, i.e., the number of molecules per surface unit cell of size A , as a function of time in Fig. 2(a). The density increases monotonously for all adsorption rates. This monotonic, yet nonlinear, behavior is consistent with a rate-equation approach introduced below. In the subsequent plots, we therefore replace the time axis by a density axis (adjusted to the adsorption rate considered).

Figure 2(b) gives insight into the orientational ordering at small adsorption rates by depicting separately the density of standing and lying molecules. Initially, the majority of molecules lies on the substrate (with preference to the x direction as supported by the ZnO charge lines), until $t \approx 3000(\nu^{\text{d}})^{-1}$. Then, the fraction of standing molecules starts to dominate, and at large times (high density) all molecules stand. The implications for cluster growth are discussed in Ref. [31], Sec. IV, where we also estimate the critical cluster size for the lying-standing transition (≈ 15 molecules). Both the lying and the standing configurations correspond to equilibrium states (determined at $f = 0$ and $r^{\text{d}} = 0$ by scaling the lattice constants) at low and high densities, respectively [15]. Moreover, the observation that molecules initially lie and later stand during thin film growth closely resembles experimental findings for self-assembled monolayers of decanethiol on silver [37]: Orientationally sensitive scattering measurements show that the first adsorbed molecules nearly immediately form a lying

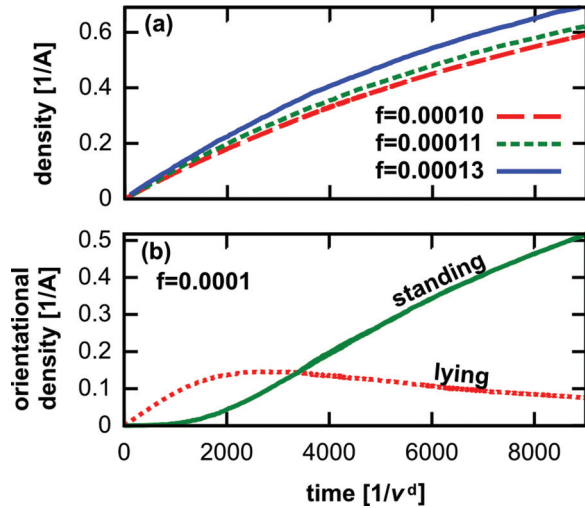


FIG. 2. Growth properties as a function of time for different adsorption rates f . (a) depicts the overall density of molecules while (b) shows the densities of standing and lying molecules as a function of time. Each molecule with $|\vartheta_i| \leq 0.25\pi$ is classified as standing.

phase, which, as the density increases, transforms to a standing phase [37–39]. This orientational reordering appears to be generic for a wide class of material combinations [9,22,38–40] and only very strongly attractive substrates do not support a transition to a standing molecular orientation [39].

The dependency of the orientational ordering on the rate of adsorption is analyzed in Fig. 3, where we plot S and B as functions of density for several values of f (including $f = 0$). An overview over different f and densities is given in Fig. 4. Apart from statistical fluctuations, the data do not depend on the system size.

In equilibrium, the system displays two transitions [see Fig. 3(a)]: first, from nematic (lying) to a biaxial phase where

the molecules orient either along the charge lines or the z axis (at a density of $\approx 0.26 \text{ \AA}^{-1}$) or along the z axis (standing); and, second, from biaxial to full nematic standing at $\approx 0.41 \text{ \AA}^{-1}$.

We now turn to nonequilibrium effects. For low, yet nonzero, adsorption rates ($f = 0.0001$), molecules have less time to form a nematic lying order. As a consequence, both the transition from lying to biaxial and the transition from biaxial to standing nematic move towards lower densities. For very high adsorption rates ($f = 0.01$), the standing order initiated through molecule adsorption dominates the orientational ordering throughout the growth process, as depicted in Fig. 3(c). Here, the nematic order parameter S never assumes negative values and the biaxiality parameter never is significantly larger than zero. The intermediate range is dominated by competition of various morphologies, exemplified for $f = 0.001$ in Fig. 3(c). Initially, the standing orientation dominates. Then, the system transitions to biaxial at $\approx 0.02 \text{ \AA}^{-1}$ and lying nematic at $\approx 0.078 \text{ \AA}^{-1}$, as the initially adsorbed molecules lie down. With increasing molecule density, the molecular morphology observed in equilibrium becomes more significant. Correspondingly, the transition from lying to biaxial, and from biaxial to standing, resemble the transitions seen for $f = 0.0001$ in Figs. 3(a) and 3(b), except that they are shifted to lower densities. We call this phenomenon “reentrant” growth, because the initial standing orientation vanishes, but reoccurs during the final stages of growth.

The rate dependency of the collective orientation behavior is summarized in Fig. 4 for a range of adsorption rates and associated densities.

Here, three interesting features become apparent. First, there is reentrant growth for intermediate adsorption rates close to $f = 0.001$, as discussed above. Second, the transitions of $S(f)$ (marked in Fig. 4) are nonmonotonous with f . This observation is verified by multiple runs for $0.005 \leq f \leq 0.0005$ for lattices with between 2500 and 10^6 lattice sites.

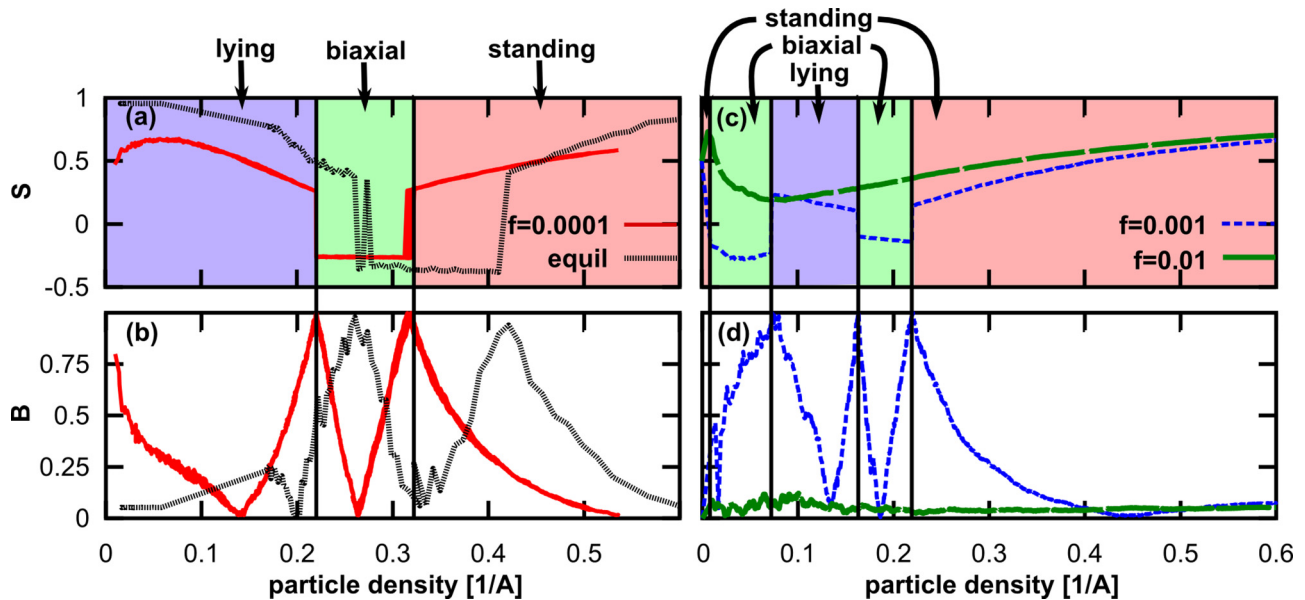


FIG. 3. Orientational order parameters as a function of density. (a), (c) Nematic order parameter S ; (b), (d) biaxiality parameter B as functions of the molecule density for different f . (a) and (c) have underlying color blocks that mark the different morphologies arising for $f = 0.0001$ and $f = 0.001$, respectively. The vertical lines mark the transitions between these morphologies. The transitions in equilibrium and at $f = 0.01$ are not explicitly marked.

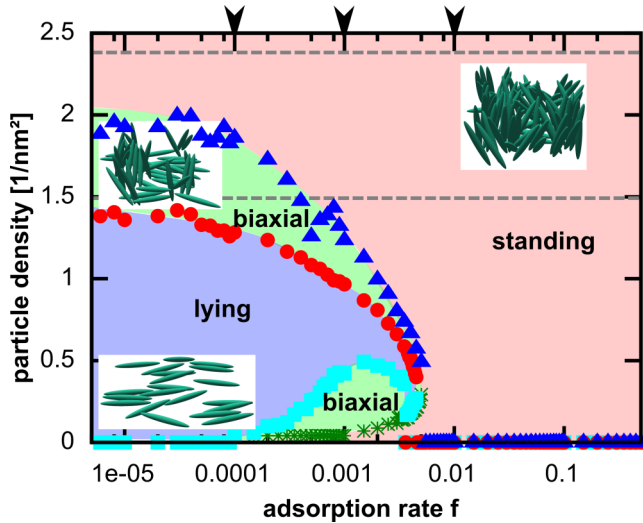


FIG. 4. “Growth state diagram” as a function of adsorption rate and density for vertically adsorbed molecules. Regions of different orientations are separated through transition points that correspond to a change in sign of S , as exemplified in Fig. 3. The dashed gray horizontal lines mark the transitions expected in equilibrium [see Fig. 3(b)]. Note that the density is here expressed in units of nm^{-2} (contrary to Fig. 3). The snapshots correspond to the lying, biaxial, and standing configurations for $f = 0.0001$, which correspond to molecule densities 0.39 , 1.59 , and 3.2 nm^{-2} , respectively. The arrows mark the adsorption rates shown in Fig. 3.

As a consequence, the orientational ordering at a fixed density of 0.25 nm^{-2} follows a sequence of states upon increase of f : lying, biaxial, lying, biaxial, and finally standing order. Third, there appears to be a “critical” adsorption rate $f_{\text{crit}} \approx 0.005$ beyond which no transitions occur.

To rationalize the occurrence of f_{crit} , we propose the following rate-equation model involving discretized rotational configurations [31]. Specifically, we assume that the number of vacant sites N_v , sites occupied by standing particles N_s , and sites occupied by lying particles N_l change in time according to $\dot{N}_v \equiv dN_v/dt = -N_v f$, $\dot{N}_s = N_v f - N_s r$, $\dot{N}_l = N_s r$, where r is the rate of reorientations. The transition from standing to lying is identified with the condition $N_s(t) = N_l(t)$. Solving the rate equations accordingly, we find the implicit equation $(2 - \Theta)x - 2x \exp[\ln(1 - \Theta)/x] = \Theta$, where $\Theta(t) = [N_s(t) + N_l(t)]/N$ and $x = f/r$. This yields (see Ref. [31], Sec. V) the critical adsorption rate $f'_{\text{crit}} \approx 0.0055$, in very good agreement with the corresponding

simulation result. Physically, our model demonstrates that f_{crit} results from the competition between the time scales of adsorption (f^{-1}) and reorientation (r^{-1}).

In summary, our KMC simulations of the prototypical organic-inorganic system 6P on $\text{ZnO}(10\bar{1}0)$ clearly show that nonequilibrium morphologies can be strongly different from those found for $f = 0$. The present calculations are based on spatially dependent pair potentials parametrized according to DFT results, and, unlike earlier KMC studies [18,19], we assume *continuous 3D* rotations. This allows us to explore the full complexity of nonequilibrium orientational ordering.

To which extent are the results *generic* for hybrid inorganic-organic systems? In fact, while our coarse-grained Hamiltonian (2) is designed for a specific material system (and surface temperature T), the observed competition between lying and standing orientations as a function of f is a rather universal feature [38]. Regarding surface properties, one would clearly expect an impact of T and also of the surface structure: For higher T the “orientational bias” exerted by charged stripes of $\text{ZnO}(10\bar{1}0)$ weakens, destabilizing the lying nematic phase already at $f = 0$ [15]. In nonequilibrium ($f > 0$), we thus expect the critical rate f_{crit} for vertical adsorption (and generally the regime of rates related to lying phases) to decrease. For substrate temperatures $T \lesssim 300 \text{ K}$ [41], the temperature difference between adsorbing molecules and the substrate may cause hot precursor states, which reduce the influence of T [42,43]. Similarly, inorganic surfaces without a biasing field will lead to a destabilization of biaxial phases. Regarding the molecules, decreasing their length (e.g., from 6P to 2P) reduces the anisotropy of sterical interactions even in the uncharged case [38]; thus, lying phases can exist up to higher densities [44]. For quadrupolar molecules, shorter lengths weaken the electrostatic substrate interactions [4], so we again expect f_{crit} to decrease.

The understanding of these different, nonequilibrium molecular structures forms an important ingredient for later calculations of optical behavior. Hence, our understanding of the collective ordering during growth of hybrid structures contributes to the creation of greener, more sustainable, and cost-efficient optoelectronic devices [45–47]. We hope that our simulation results stimulate further experiments in this direction.

This work was supported by the Deutsche Forschungsgemeinschaft within CRC 951 (Project A7). We acknowledge interesting discussions with M. Klopotek, F. Schreiber, and M. Oettel.

[1] M. Law, L. Greene, J. Johnson, R. Saykally, and P. Yang, *Nat. Mater.* **4**, 455 (2005).
 [2] C.-Y. Liu, Z. C. Holman, and U. R. Kortshagen, *Nano Lett.* **9**, 1 (2009).
 [3] J. J. Rindermann, G. Pozina, B. Monemar, L. Hultman, H. Amano, and P. G. Lagoudakis, *Phys. Rev. Lett.* **107**, 236805 (2011).
 [4] S. Blumstengel, S. Sadofev, C. Xu, J. Puls, and F. Henneberger, *Phys. Rev. Lett.* **97**, 237401 (2006).

[5] Y. Vaynzof, A. A. Bakulin, S. Gélinas, and R. H. Friend, *Phys. Rev. Lett.* **108**, 246605 (2012).
 [6] Y. Xu, O. T. Hofmann, R. Schlesinger, S. Winkler, J. Frisch, J. Niederhausen, A. Vollmer, S. Blumstengel, F. Henneberger, N. Koch, P. Rinke, and M. Scheffler, *Phys. Rev. Lett.* **111**, 226802 (2013).
 [7] R. Schlesinger, F. Bianchi, S. Blumstengel, C. Christodoulou, R. Ovsyannikov, B. Kobin, K. Moudgil, S. Barlow, S. Hecht, S. R. Marder, F. Henneberger, and N. Koch, *Nat. Commun.* **6**, 6754 (2015).

- [8] S. Braun, W. Osikowicz, Y. Wang, and W. R. Salaneck, *Org. Electron.* **8**, 14 (2007).
- [9] G. Hlawacek and C. Teichert, *J. Phys.: Condens. Matter* **25**, 143202 (2013).
- [10] E. Zojer, N. Koch, P. Puschnig, F. Meghdadi, A. Niko, R. Resel, C. Ambrosch-Draxl, M. Knupfer, J. Fink, J. L. Brédas, and G. Leising, *Phys. Rev. B* **61**, 16538 (2000).
- [11] C. Simbrunner, *Semicond. Sci. Technol.* **28**, 053001 (2013).
- [12] S. Blumstengel, H. Glowatzki, S. Sadofev, N. Koch, S. Kowarik, J. P. Rabe, and F. Henneberger, *Phys. Chem. Chem. Phys.* **12**, 11642 (2010).
- [13] M. Sparenberg, A. Zykov, P. Beyer, L. Pithan, C. Weber, Y. Garmshausen, F. Carla, S. Hecht, S. Blumstengel, F. Henneberger, and S. Kowarik, *Phys. Chem. Chem. Phys.* **16**, 26084 (2014).
- [14] C. Simbrunner, D. Nabok, G. Hernandez-Sosa, M. Oehzelt, T. Djuric, R. Resel, L. Romaner, P. Puschnig, C. Ambrosch-Draxl, I. Salzmann, G. Schwabegger, I. Watzinger, and H. Sitter, *J. Am. Chem. Soc.* **133**, 3056 (2011).
- [15] N. Kleppmann and S. H. L. Klapp, *J. Chem. Phys.* **142**, 064701 (2015).
- [16] F. Della Sala, S. Blumstengel, and F. Henneberger, *Phys. Rev. Lett.* **107**, 146401 (2011).
- [17] P. A. Golubkov and P. Ren, *J. Chem. Phys.* **125**, 064103 (2006).
- [18] S. F. Hopp and A. Heuer, *J. Chem. Phys.* **136**, 154106 (2012).
- [19] J. S. Raut and K. A. Fichthorn, *J. Chem. Phys.* **108**, 1626 (1998).
- [20] J. S. Raut and K. A. Fichthorn, *J. Chem. Phys.* **110**, 587 (1999).
- [21] R. Ruiz, D. Choudhary, B. Nickel, T. Toccoli, K.-C. Chang, A. C. Mayer, P. Clancy, J. M. Blakely, R. L. Headrick, S. Iannotta, and G. G. Malliaras, *Chem. Mater.* **16**, 4497 (2004).
- [22] D. Choudhary, P. Clancy, R. Shetty, and F. Escobedo, *Adv. Func. Mater.* **16**, 1768 (2006).
- [23] P. K. Jana and A. Heuer, *J. Chem. Phys.* **138**, 124708 (2013).
- [24] Y. Cao, H. Li, and L. Petzold, *J. Chem. Phys.* **121**, 4059 (2004).
- [25] S. Plimpton, C. Battaile, M. Chandross, L. Holm, A. Thompson, V. Tikare, G. Wagner, E. Webb, X. Zhou, C. Garcia Cardona, and A. Slepoy, Crossing the Mesoscale No-Mans Land via Parallel Kinetic Monte Carlo, Sandia National Laboratory Report No. SAND2009-6226, 2009 (unpublished).
- [26] A. Chatterjee and D. G. Vlachos, *J. Comput.-Aided Mater. Des.* **14**, 253 (2007).
- [27] C. Gray and K. Gubbins, *Theory of Molecular Fluids: I: Fundamentals*, International Series of Monographs on Chemistry (Oxford University Press, Oxford, U.K., 1984).
- [28] J. G. Gay and B. J. Berne, *J. Chem. Phys.* **74**, 3316 (1981).
- [29] D. J. Cleaver, C. M. Care, M. P. Allen, and M. P. Neal, *Phys. Rev. E* **54**, 559 (1996).
- [30] J.-P. Hansen and I. R. McDonald, *Theory of Simple Liquids*, 2nd ed. (St. Edmundsbury Press Limited, Bury St. Edmunds, Suffolk, 1990).
- [31] See Supplemental Material at <http://link.aps.org/supplemental/10.1103/PhysRevB.94.241404> for details on the methods used and additional robustness calculations.
- [32] K. Palczynski and J. Dzubiella, *J. Phys. Chem. C* **118**, 26368 (2014).
- [33] P. Allen and D. Tildesley, *Computer Simulation of Liquids* (Clarendon, Oxford, U.K., 1989).
- [34] D. A. Strehober, H. Engel, and S. H. L. Klapp, *Phys. Rev. E* **88**, 012505 (2013).
- [35] D. Andrienko, M. P. Allen, G. Skačej, and S. Žumer, *Phys. Rev. E* **65**, 041702 (2002).
- [36] D. Andrienko (unpublished).
- [37] F. Schreiber, A. Eberhardt, T. Y. B. Leung, P. Schwartz, S. M. Wetterer, D. J. Lavrich, L. Berman, P. Fenter, P. Eisenberger, and G. Scoles, *Phys. Rev. B* **57**, 12476 (1998).
- [38] F. Schreiber, *Prog. Surf. Sci.* **65**, 151 (2000).
- [39] W. Brütting, *Physics of Organic Semiconductors* (Wiley, Hoboken, NJ, 2006).
- [40] T. Potocar, S. Lorbek, D. Nabok, Q. Shen, L. Tumbek, G. Hlawacek, P. Puschnig, C. Ambrosch-Draxl, C. Teichert, and A. Winkler, *Phys. Rev. B* **83**, 075423 (2011).
- [41] A. Winkler, *Surf. Sci.* **652**, 367 (2016).
- [42] A. Winkler and L. Tumbek, *J. Phys. Chem. Lett.* **4**, 4080 (2013).
- [43] J. R. Morales-Cifuentes, T. L. Einstein, and A. Pimpinelli, *Phys. Rev. Lett.* **113**, 246101 (2014).
- [44] M. Klopotek and M. Oettel (private communication).
- [45] C. R. Kagan, D. B. Mitzi, and C. D. Dimitrakopoulos, *Science* **286**, 945 (1999).
- [46] C. Raimondo, N. Crivillers, F. Reinders, F. Sander, M. Mayor, and P. Samori, *Proc. Natl. Acad. Sci. USA* **109**, 12375 (2012).
- [47] M. E. Roberts, S. C. B. Mannsfeld, N. Queralto, C. Reese, J. Locklin, W. Knoll, and Z. Bao, *Proc. Natl. Acad. Sci. USA* **105**, 12134 (2008).